Available online at www.sciencedirect.com

SCIENCE DIRECT®

Remote Sensing of Environment 92 (2004) 181–194

Remote Sensing of Environment

www.elsevier.com/locate/rse

Nighttime polar cloud detection with MODIS

Yinghui Liu[a,*], Jeffrey R. Key[b], Richard A. Frey[a], Steven A. Ackerman[a], W. Paul Menzel[b]

[a] *Department of A.O.S., Cooperative Institute for Meteorological Satellite Studies, University of Wisconsin-Madison, 1225 West Dayton Street, Madison, WI 53706, USA*

[b] *Office of Research and Applications, NOAA/NESDIS, Madison, WI, USA*

Received 21 January 2004; received in revised form 27 May 2004; accepted 3 June 2004

Abstract

Cloud detection is the first step in studying the role of polar clouds in the global climate system with satellite data. In this paper, the cloud detection algorithm for the Moderate Resolution Imaging Spectrometer (MODIS) is evaluated with model simulations and satellite data collocated with radar/lidar observations at three Arctic and Antarctic stations. Results show that the current MODIS cloud mask algorithm performs well in polar regions during the day but does not detect more than 40% of the cloud cover over the validation sights at night. Two new cloud tests utilizing the 7.2 μm water vapor and 14.2 μm carbon dioxide bands, one new clear-sky test using the 7.2 μm band, and changes to the thresholds of several other tests are described. With the new cloud detection procedure, the misidentification of cloud as clear decreases from 44.2% to 16.3% at the two Arctic stations, and from 19.8% to 2.7% at the Antarctic station.
© 2004 Elsevier Inc. All rights reserved.

Keywords: Polar; Cloud detection; MODIS

1. Introduction

The variation of cloud amount over the polar regions strongly influences planetary albedo gradients and surface energy exchanges (Key & Barry, 1989), which, in turn, affect regional and global climate (Curry et al., 1996). While cloud radiative properties are important in the study of clouds in polar climate systems, the first step is to determine when and where clouds exist. Limited surface observations of cloud cover in the Arctic and Antarctic makes the use of satellite data necessary. However, the detection of polar clouds is inherently difficult due to poor thermal and visible contrast between clouds and the underlying snow/ice surface, small radiances from the cold polar atmosphere, and ubiquitous temperature and humidity inversions in the lower troposphere (Lubin & Morrow, 1998).

Polar cloud detection from remote sensing data has been an area of active research during the past decade (Gao et al., 1998). The International Satellite Cloud Climatology Project (ISCCP) employs a combination of spectral, temporal, and spatial tests to estimate clear-sky radiances and values of cloud forcing (Key & Barry, 1989; Rossow & Garder, 1993; Rossow & Schiffer, 1991; Rossow et al., 1993) and increases the sensitivity of low-level cloud detection over snow and ice in polar regions by use of a new threshold test on 3.7 μm radiances (Rossow & Schiffer, 1999). The TOVS Polar Pathfinder cloud detection scheme uses a series of spectral tests to determine if a pixel is clear or cloudy (Schweiger et al., 1999). Statistical classification procedures, including maximum likelihood and Euclidean distance methods, have been applied in cloud detection algorithms (Ebert, 1989; Key, 1990; Key et al., 1989; Welch et al., 1988, 1990, 1992). Single- and bispectral threshold methods have been developed and applied to polar data (Ackerman, 1996; Gao et al., 1998; Inoue, 1987a, 1987b; Minnis et al., 2001; Spangenberg et al., 2001, 2002; Yamanouchi et al., 1987).

The Moderate Resolution Imaging Spectrometer (MODIS) on the NASA Terra and Aqua satellites provides an unprecedented opportunity for earth remote sensing. Its broad spectral range (36 bands between 0.415–14.235 μm), high spatial resolution (250 m for 5 bands, 500 m for 5 bands, and 1000 m for 29 bands), frequent observations of polar regions (28 times a day), and low thermal band instrument noise (roughly 0.1 K for a 300 K scene) provide a number of possibilities for improving cloud detection.

* Corresponding author. Tel.: +1-608-265-8620; fax: +1-608-262-5974.

E-mail address: yinghuil@ssec.wisc.edu (Y. Liu).

0034-4257/$ - see front matter © 2004 Elsevier Inc. All rights reserved.
doi:10.1016/j.rse.2004.06.004

The goal of this study is to present improvements to the MODIS cloud mask algorithm for the detection of polar clouds at night. Changes to some of the current spectral tests are recommended, and new tests are proposed. The physical basis for these tests are described and supported by radiative transfer simulations. Validation of the satellite-derived cloud detection results is accomplished with surface-based cloud radar and lidar data from Alaska and the South Pole. It will be shown that nighttime cloud detection in polar regions with MODIS can achieve a high level of accuracy and is far more robust than what may be obtained with the Advanced Very High Resolution Radiometer (AVHRR). These enhancements will be incorporated into the next version of the NASA MODIS cloud mask.

2. Data and radiative transfer model

MODIS scans a swath width sufficient for providing global coverage every 2 days from a polar-orbiting, sun-synchronous platform at an altitude of 705 km (King et al., 2003; Platnick et al., 2003). The MODIS Level 1B (MOD021KM) data product contains calibrated radiances for all 36 MODIS spectral bands at 1 km resolution. The MODIS geolocation data (MOD03) contain geodetic latitude and longitude, surface height above geoid, solar zenith and azimuth angles, satellite zenith and azimuth angles, and a land/sea mask for each 1-km sample. The MODIS products, including MOD021KM, MOD03, and the cloud mask (MOD35), were obtained from the NASA Goddard Space Flight Center Distributed Active Archive Center (GDAAC).

The U.S. Department of Energy's Atmospheric Radiation Measurement (ARM) program collects data at two polar sites, both in Alaska: the North Slope of Alaska (NSA) at Barrow and Atqasuk. These sites provide cloud information with a Vaisala Ceilometer (VCEIL), a Millimeter Wave Cloud Radar (MMCR), and a Micropulse Lidar (MPL) at Barrow and a VCEIL at Atqasuk. An MPL is also operated by the National Oceanic and Atmospheric Administration (NOAA) Climate Monitoring and Diagnostics Laboratory at the South Pole Atmospheric Observatory. Accurate cloud boundary information and fraction of cloud occurrence can be derived from the radar, lidar, or/and combination of radar and lidar measurements (Campbell et al., 2002; Clothiaux et al., 2000; Intrieri et al., 2002).

The Active Remote Sensing of Clouds (ARSCL) product combines data from MMCR, MPL, and VCEIL instruments to produce a time series of the vertical distribution of cloud hydrometeors (Clothiaux et al., 2000). This value-added product provides clear/cloudy discrimination, cloud bottom, and cloud top height for up to 10 layers at Barrow. The temporal and vertical spatial resolution of this product is 10 s and 45 m, and the vertical range is up to 20 km. At Atqasuk, the VCEIL data provide clear/cloudy discrimination and cloud base height for up to three layers. The temporal and vertical spatial resolution of this product is 15 s and 30 m, and the vertical range is up to 75,000 m. The MPL data at the South Pole are obtained from the NASA Micro-Pulse Lidar Network (MPLNET). There is no operational cloud mask product with these observations at the South Pole. We use a simple threshold method to identify clouds at South Pole: When the normalized relative backscatter of the MPL observation is larger than a threshold of 0.3, it is labeled as cloudy. Cloud mask products at Barrow and Atqasuk in 2001 and 2002 and at the South Pole in 2001 were assembled to match MODIS overpass times. These are collectively referred to as the radar/lidar cloud product in the remainder of the paper.

The following method is used to match the radar/lidar cloud product to MODIS cloud mask data. For each MODIS observation (pixel) over Barrow or Atqasuk, 5 min of cloud mask data from radar/lidar, centered at the exact MODIS overpass time, is used to determine the cloud fraction; that is, the radar/lidar cloud fraction is a temporal rather than a spatial average. When the fraction of cloud occurrence is larger than 95%, it is considered cloudy; it is clear when the value is less than 5%.

The use of cloud radar and lidar for cloud detection is not always straightforward, as MODIS, radar, and lidar have different sensitivities to cloud particles. For example, previous studies (e.g., Intrieri et al., 2002) have shown that lidar is very sensitive to thin clouds, probably much more sensitive than MODIS is. Using a simple threshold to determine whether a cloud is in the lidar field of view at South Pole sets a bound on what we define as cloud. Overall, we would expect that radar/lidar would give greater cloud amounts than MODIS does, particularly for high, thin clouds. As will be shown later, this may be the case, especially for the current MODIS cloud mask algorithm, as there are many high clouds detected by radar/lidar but not by MODIS. The available data do not allow

Table 1
Meteorological stations used in this study

Station ID (WMO #)	Latitude	Longitude	Station elevation (m)	Station
Barrow	71.32	− 156.62	3	Barrow
89002	− 70.67	− 8.25	40	Neumayer
89022	− 75.5	− 26.65	30	Halley
89532	− 69.0	39.58	21	Syowa
02185	65.55	22.13	16	Lulea/Kallax
20674	73.53	80.40	47	Ostrov Dikson
21824	71.58	128.92	8	Tiksi
21946	70.62	147.90	61	Cokurdah
22113	68.97	33.05	51	Murmansk
22217	67.15	32.35	26	Kandalaksa
24125	68.50	112.43	220	Olenek
24266	67.55	133.38	137	Verhojansk

Latitudes are positive north of the equator; longitudes are positive east of the prime Meridian.

Table 2
Tests used in the current MODIS cloud mask algorithm for polar regions

	Nighttime snow/ice	Nighttime land	Nighttime ocean	Daytime snow/ice	Daytime land	Daytime ocean	Antarctica daytime land
BT11			✓			✓	
BT6.7	✓	✓	✓	✓	✓	✓	✓
BT3.9-BT12	✓	✓		✓			✓
BT11-BT3.9	✓	✓	✓		✓	✓	
BT8.7-BT11			✓			✓	
BT11-BT12		✓	✓		✓	✓	
R0.66 or R0.86					✓	✓	
R0.86/R0.66					✓	✓	
R1.38				✓ (low elevation)	✓	✓	
Spatial test		✓	✓				
BT6.7-BT11	✓						

BTx is the brightness temperature at wavelength x (microns), and Rx is the reflectance at wavelength x (microns).

us to evaluate errors based on cloud optical thickness. Differences in cloud detection for surface-based instruments and MODIS are discussed in detail in Berendes et al. (2004; "Cloud cover comparisons of MODIS daytime cloud mask with surface instruments at the north slope of Alaska ARM site", submitted to IEEE Transactions on Geoscience and Remote Sensing).

Radiosonde data provide vertical profiles of temperature, humidity, and winds. The times of the radiosonde data do not always match those of the MODIS overpasses, hence, only those within 1-h MODIS are used. Data were obtained from the NOAA Forecast System Laboratory in 2001 and 2002 for nine meteorological stations in the Arctic and three in the Antarctic (Table 1).

To illustrate the physical principles upon which the spectral tests are based, MODIS brightness temperatures are simulated with the radiative transfer model Streamer (Key & Schweiger, 1998). For radiance calculations, Streamer utilizes a discrete ordinate solver. Its 24 shortwave bands cover the spectral interval from 0.28 to 4.0 μm; the 105 longwave bands cover the spectral range from 4.03 to 500 μm. The MODIS spectral response functions for each band are incorporated in the calculations, albeit coarsely. For ice clouds in the shortwave, there are variety of ice crystal shapes or "habits", which include hexagonal solid columns, hexagonal hollow columns, rough aggregates, bullet rosettes with four branches, bullet rosettes with two to six branches, plates, dendrites, and spherical particles. For ice clouds in the longwave, spherical particles are used, with optical properties based on Mie calculations, parameterized in terms of the particle effective radius and water content. Streamer provides seven standard atmospheric profiles, which include tropical, midlatitude summer, midlatitude winter, subarctic summer, subarctic winter, arctic summer, and arctic winter. The Arctic profiles of temperature and humidity are based on Arctic Ocean coastal and drifting station data.

3. Current MODIS cloud mask algorithm

In the MODIS cloud mask algorithm (Ackerman et al., 1998), the polar regions are treated as one of several domains defined according to latitude, surface type, and solar illumination, including land, water, snow/ice, desert, and coast for both day and night. A series of spectral tests is applied to identify the presence of clouds. There are several groups of tests, with differing numbers of tests in

Table 3
Comparison between radar/lidar and the current MODIS cloud mask results in the polar regions

Category	Radar/lidar	MODIS	Arctic daytime	Arctic nighttime	Antarctica daytime	Antarctic nighttime
1	Cloud	Cloud	359	412	118	331
2	Cloud	Uncertain clear	4	9	2	31
3	Cloud	Probably clear	25	99	15	9
4	Cloud	Confident clear	10	327	12	82
5	Clear	Confident clear	81	205	113	217
6	Clear	Probably clear	6	37	29	0
7	Clear	Uncertain clear	6	6	15	0
8	Clear	Cloud	6	18	29	0
Rate 1 (%)			2.7	44.2	9.2	19.8
Rate 2 (%)			6.9	8.1	20.4	0.0

Rate 1 is the MODIS misidentification rate of cloud as clear, which is the ratio of the number of category-4 cases to the number of cases in categories 1 and 4. Rate 2 is the MODIS misidentification rate of clear as cloud, defined as the ratio of the number of category-8 cases to the number of cases in categories 5 and 8.

each group, depending on the domain. A clear-sky confidence level ranging from 1 (high) to 0 (low) is returned for each test. The minimum confidence from all tests within a group is taken to be representative of that group. The Nth root of the product of all the group confidences (Q) determines the final confidence, where N is the number of groups. The four confidence levels included in the cloud mask output are confident clear (Q>0.99), probably clear (Q>0.95), uncertain/probably cloudy (Q>0.66), and cloudy ($Q \leq 0.66$). MODIS Level 2 cloud mask data (MOD35) contains the final confidence levels for each 1-km sample. The tests for different domains are listed in Table 2.

To validate the current MODIS cloud mask algorithm in polar regions, we use cloud mask results from radar/lidar observations as truth. In the MODIS cloud mask, there are four conditions: confident clear, probably clear, uncertain, and cloudy, although the radar/lidar mask yields only clear or cloudy. Therefore, each matched alradar/lidar and MODIS cloud mask pair for Barrow, Atqasuk, and South Pole will be in one of eight categories, as shown in Table 3. We can further divide the results into low-altitude (Barrow and Atqasuk) and high-altitude (South Pole) groups. Table 3 lists the frequency of observations in each of the eight categories. In the table, the Arctic refers to the two Alaska locations and the Antarctic refers to South Pole. The misidentification rate will be used to evaluate the cloud mask results. The misidentification rate of cloud as clear is defined as the ratio of the number of category-4 cases to the number of cases in categories 1 and 4 (shown as "Rate 1" in Tables 3–6). The misidentification rate of clear as cloud is defined as the ratio of the number of category-8 cases to the number of cases in categories 5 and 8 (shown as "Rate 2" in Tables 3–6).

For the MODIS cloud mask during the sunlit portion of the year/day (solar zenith angle less than 80°; hereafter "day" or "daytime") in the Arctic, as shown in Table 3, we find that 2.7% of the cloudy cases identified by radar/lidar are misidentified as clear in the MODIS cloud mask, and 6.9% of the clear cases identified by radar/lidar are misidentified as cloud. At South Pole, 9.2% of the cloud identified by radar/lidar is misidentified as clear by MODIS cloud mask, and 20.4% of the clear identified by radar/lidar is misidentified as cloud.

At night in the Arctic, 44.2% of the cloud identified by radar/lidar is misidentified as clear, and 8.1% of the clear identified by radar/lidar is misidentified as cloud. In the Antarctic, 19.8% of the cloud identified by radar/lidar is misidentified as clear, while no clear identified by radar/lidar is misidentified as cloud in the MODIS cloud mask.

Tables 4 and 5 show the effect of cloud top height and the number of cloud layers, respectively, on cloud detection in the current nighttime cloud mask algorithm for the Arctic. The tables give the number of observations for the various combinations of radar/lidar and MODIS detection; for example, 51 high cloud cases were labeled cloudy by both the radar/lidar and MODIS, and 45 were labeled cloudy by radar/lidar but clear by MODIS. One reason for some cases that are detected as cloud by radar/lidar but as clear by MODIS may be the difference in the detection ability of radar/lidar and MODIS; for example, radar/lidar

Table 4
The effect of cloud top height on cloud detection using MODIS at nighttime, where values indicate the number of cases labeled cloudy by radar/lidar, cloudy or clear by MODIS in the current and modified (in parentheses) algorithms

Radar/Lidar	MODIS	High cloud	Middle cloud	Low cloud
Cloud	Cloud	51 (87)	43 (133)	167 (221)
Cloud	Uncertain	5 (10)	3 (5)	0 (12)
Cloud	Probably clear	13 (1)	27 (0)	19 (1)
Cloud	Confident clear	45 (16)	87 (22)	99 (51)
Total		114	160	285
Rate 1 (%)		46.9 (15.5)	66.9 (14.2)	37.2 (18.8)

Rate 1 is as defined for Table 3.

Table 5
The effect of the number of cloud layers on cloud detection using MODIS at nighttime, where values indicate the number of cases labeled cloudy by radar/lidar, cloudy and clear by MODIS in the current and modified (in parentheses) algorithms

Radar/Lidar	MODIS	One-layer	Two-layer	Three-layer
Cloud	Cloud	308 (463)	76 (152)	28 (56)
Cloud	Uncertain	2 (23)	4 (10)	3 (5)
Cloud	Probably clear	61 (6)	28 (0)	10 (1)
Cloud	Confident clear	217 (96)	77 (23)	33 (12)
Total		588	185	74
Rate 1 (%)		41.3 (17.2)	50.3 (13.1)	54.1 (17.6)

Rate 1 is as defined for Table 3.

Table 6
Comparison of the modified and current (in parentheses) cloud mask algorithms in the Arctic and Antarctic at night

Radar/Lidar	MODIS	Arctic nighttime (MODIS)	Arctic nighttime (AVHRR)	Antarctic nighttime (MODIS)	Antarctic nighttime (AVHRR)
Cloud	Cloud	671 (412)	492	439 (331)	409
Cloud	Uncertain	38 (9)	42	2 (31)	18
Cloud	Probably clear	7 (99)	10	0 (9)	2
Cloud	Confident clear	131 (327)	303	12 (82)	24
Clear	Confident clear	223 (205)	230	208 (217)	0
Clear	Probably clear	4 (37)	7	0 (0)	0
Clear	Uncertain	18 (6)	15	1 (0)	0
Clear	Cloud	21 (18)	14	8 (0)	217
Rate 1 (%)		16.3 (44.2)	38.1	2.7 (19.8)	5.5
Rate 2 (%)		8.6 (8.1)	5.7	3.7 (0.0)	100.

Rates 1 and 2 are as defined for Table 3.

has greater sensitivity to high, thin clouds than MODIS does. The numbers shown in the parentheses are the results after the modified cloud mask algorithm is applied, as described in the next section. The cloud top height data in Table 4 are only available at Barrow. The values in Table 5 are for both Barrow and Atqusak. The tables show that the misidentification rate of cloud as clear by MODIS is greatest for middle cloud and multiple layers, and least for low cloud and single layers in the current cloud mask algorithm.

In the current MODIS cloud mask algorithm for nighttime in polar region over land and snow/ice, four cloud detection tests, including BT6.7, BT11-BT3.9, BT3.9-BT12, and BT11-BT12, and one clear detection test, BT6.7-BT11, are used, where "BT" stands for brightness temperature and the number is the wavelength, in microns. These will now be described in greater detail. Thresholds for the various tests are not given here but are available from the authors.

3.1. The BT6.7 cloud test

Fig. 1 shows that in clear-sky conditions, the weighting function of the 6.7 μm band calculated for the subarctic winter standard atmosphere peaks at about 600 hPa; hence, the brightness temperature, BT6.7, is related to the temperature near 600 hPa. When thick a cloud higher than 600 hPa is present, BT6.7 is related to the temperature at the cloud top rather than the temperature at 600 hPa. The temperature at the top of a high, thick cloud will be lower than the temperature at 600 hPa, which leads to a lower BT6.7 compared with clear conditions. A threshold is set for this test, and when the observed BT6.7 is lower than this value, the pixel is labeled cloudy.

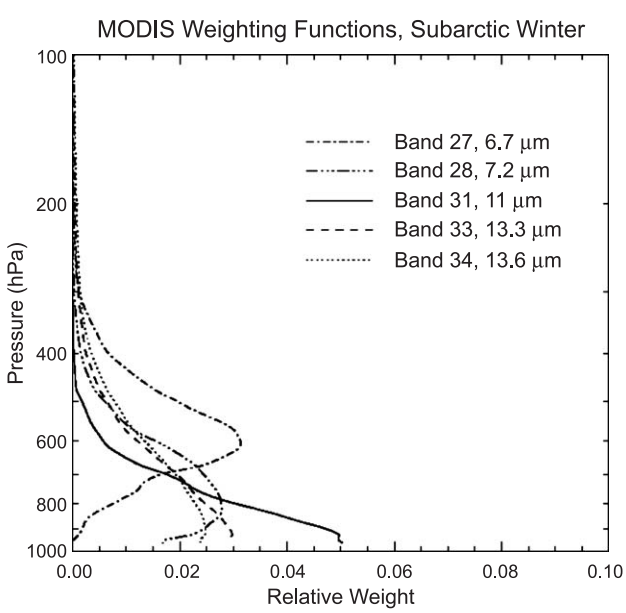

Fig. 1. Weighting functions for the MODIS bands at 6.7, 7.2, 11 μm, 13.3, and 13.6 μm using a subarctic winter standard atmosphere profile.

3.2. The BT11-BT3.9 and BT3.9-BT12 cloud tests

Simulations of BT3.9-BT11 are shown in Fig. 2(a)–(c) for ice cloud and in Fig. 2(d)–(f) for water cloud with different cloud top heights. Streamer is used to do the simulation with its standard profile for Arctic winter, which includes a temperature inversion. The cloud top heights are at 900 (low cloud), 700 (middle cloud), and 400 hPa (high cloud). Fig. 3 shows indices of refraction for ice and water from 3.5 to 15 μm (Ray, 1972; Segelstein, 1981; Warren, 1984). The real portion represents the magnitude of scattering, and the imaginary part is an indication of absorption, such that absorption by water and ice is smaller at 3.9 μm than at 11 μm, but scattering is greater.

The near-surface atmosphere in polar regions is characterized by temperature inversions throughout most of the year, especially at night. When a temperature inversion is present and the cloud top is near the inversion top, as is the case for Fig. 2(a), (b), (d), and (e), BT3.9-BT11 decreases with increasing cloud optical thickness over the range 0.1–3.0. A larger contribution from the lower layers in the clouds that have lower temperatures results in a smaller brightness temperature at 3.9 μm lower than at 11 μm. When cloud optical thickness increases beyond 2.0–3.0, the brightness temperature difference (BTD) increases then levels off due to increased scattering, with the BTD smaller for water cloud than for ice cloud. For high cloud, BT3.9-BT11 increases with increasing cloud optical thickness over the range 0.1–3.0 because the cloud is colder than the surface is, with the maximum value of 5.0 K for ice cloud and 6.0 K for water cloud.

Changes of BT3.9-BT11 for high, middle, and low clouds can be used to design cloud detection tests. A BT3.9-BT12 test is used to detect high water and ice cloud, whether a temperature inversion exists, and high, middle, and low cloud without a temperature inversion. When the observed BT3.9-BT12 is larger than the threshold, it is labeled cloudy. A BT3.9-BT12 test is used instead of a BT3.9-BT11 test because there is a larger difference in the imaginary index of refraction between 3.9 and 12 μm than between 3.9 and 11 μm. A BT11-BT3.9 test is used to detect thick cloud, whether a temperature inversion exists, and low cloud in the presence of a temperature inversion. When the observed BT11-BT3.9 is larger than the threshold, it is labeled as cloudy.

3.3. The BT11-BT12 cloud test

Under clear conditions, there is stronger water vapor continuum absorption at 12 μm than at 11 μm (Fig. 3 of Strabala et al., 1994). Consequently, BT11-BT12 is positive when viewing a clear area. In the polar regions, BT11-BT12 increases with BT11 due to atmospheric water vapor absorp-

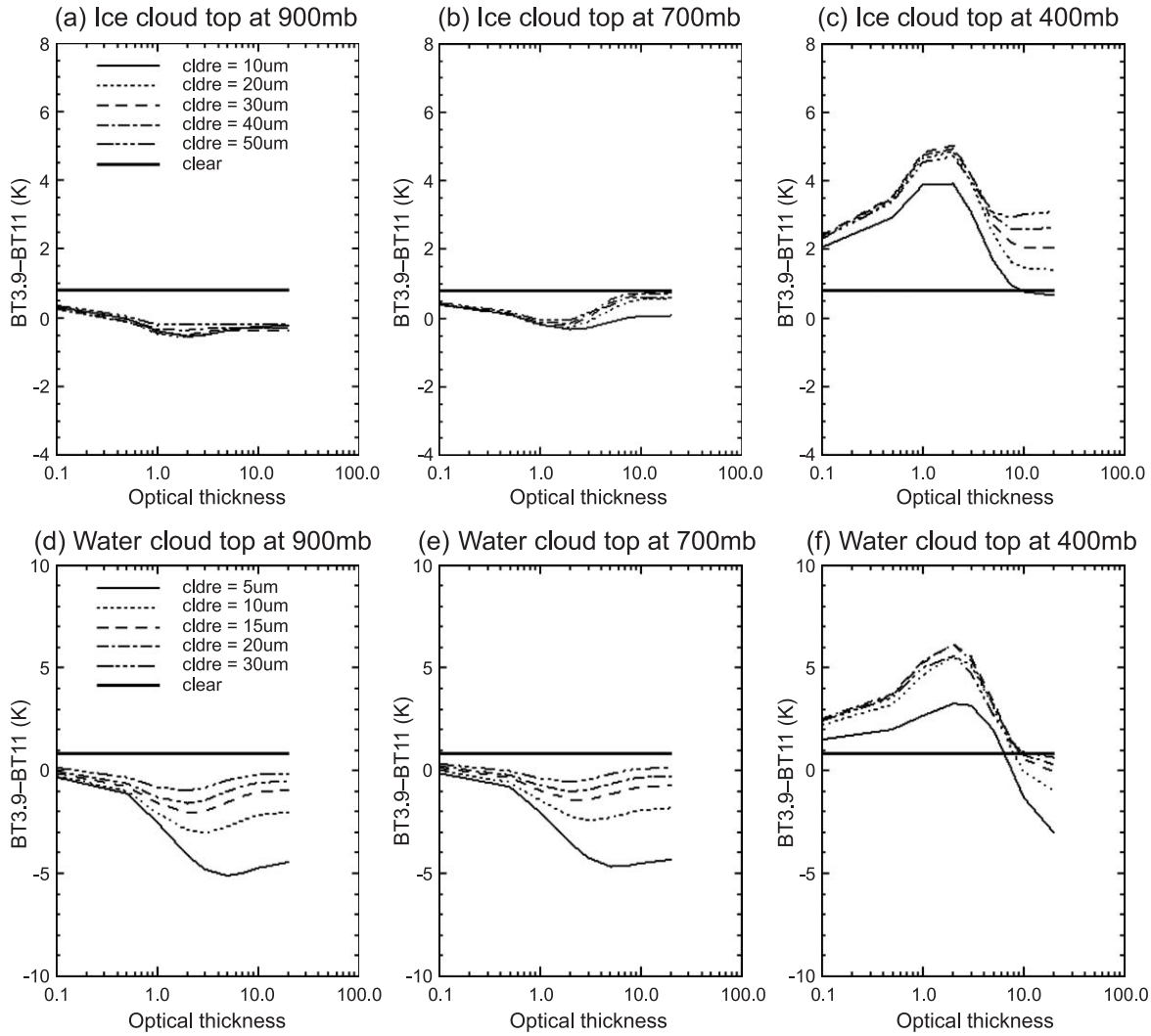

Fig. 2. Simulations of BT3.9-BT11 for ice cloud with the cloud top at (a) 900, (b) 700, and (c) 400 hPa for different ice cloud radii (cldre), and for water cloud with the cloud top at (d) 900, (e) 700, and (f) 400 hPa for different water cloud radii (cldre). An Arctic winter mean profile was used in the calculations. The temperatures at surface, 900, 700, and 400 hPa are 242, 250, 247, and 223 K, respectively.

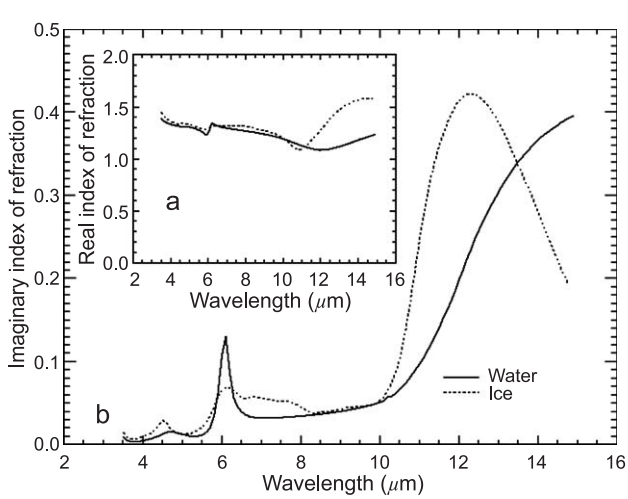

Fig. 3. Real and imaginary indices of refraction for ice and water.

tion and the difference of snow surface emissivity at 11 and 12 μm (Kadosaki et al., 2002). Based solely on the imaginary indices of refraction (Fig. 3), both water and ice absorb more at 12 μm than at 11 μm; hence, the emittance from a cloud is greater at 12 μm than at 11 μm. When the cloud is thin and the cloud is colder than the surface, BT11 is higher than BT12. When the cloud is thin and the cloud is warmer than the surface, BT11 is lower than BT12.

Thresholds for BT11-BT12 test depend on BT11 and the viewing angle due to atmospheric absorption and directional snow emissivity. In the current cloud mask algorithm, a BT11-BT12 test is only used for land and ocean surface at nighttime. For a snow/ice surface, which is inferred from the 500 m gridded MODIS snow/ice map (Ackerman et al., 1998), it is not used due to the complexity of snow/ice emissivities. Figs. 4 and 5 show different nighttime brightness temperature difference (BTD) pairs, including BT11-BT12, as a function of BT11 under clear and cloudy

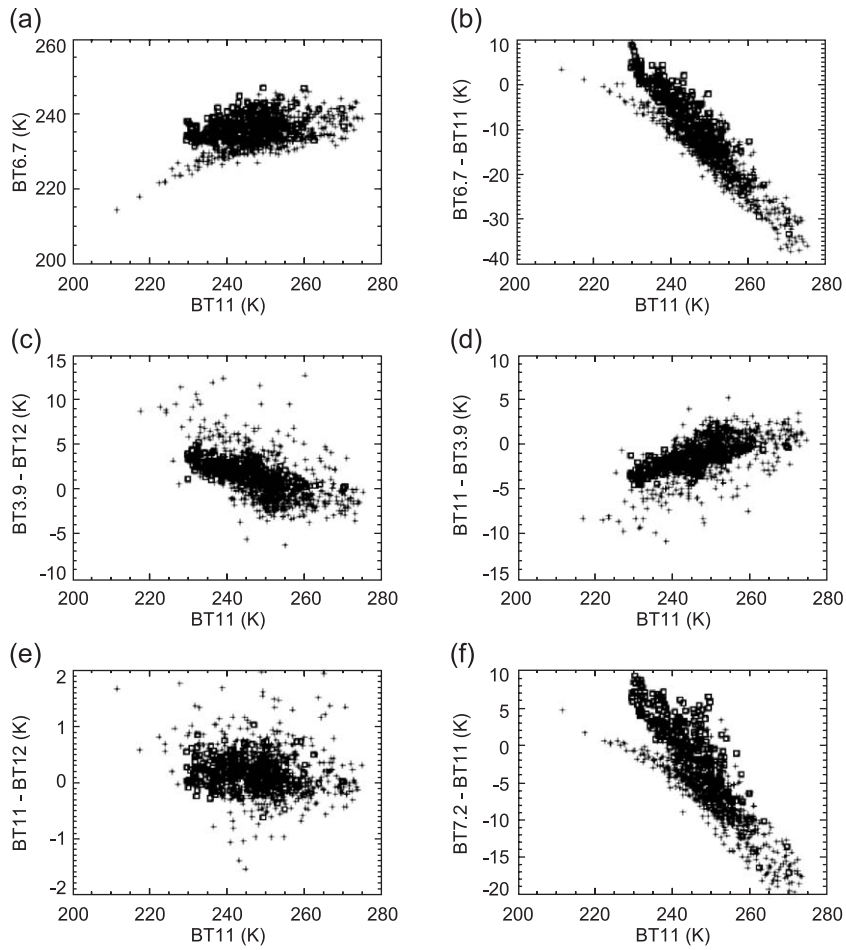

Fig. 4. (a) Observed brightness temperature at 6.7 μm and brightness temperature differences for (b) 6.7–11, (c) 3.9–12, (d) 11–3.9, (e) 11–12, and (f) 7.2–11 μm as a function of the 11-μm brightness temperature for cloudy (+) and clear (□) cases, as determined from radar/lidar data, over the Arctic at night.

conditions using matched MODIS and radar/lidar cloud mask data in the Arctic and Antarctic.

3.4. The BT6.7-BT11 clear test

Ackerman (1996) found that large negative BT11-BT6.7 differences occur in the presence of strong, low-level temperature inversions over Antarctica and that clouds inhibit the formation of the inversion and obscure the inversion from satellite detection, if the ice water path is greater than approximately 20 g m^{-2}. The BT6.7-BT11 test can therefore identify clear sky conditions when strong inversions exist. This test is used after all cloud detection tests are applied, to restore to clear for those pixels that may have been falsely labeled as cloudy. The test is most useful over the Antarctic plateau, as shown in Fig. 5(b) because of the strong surface radiation cooling.

3.5. Discussion of the current cloud tests

While the tests described above—BT6.7 for high thick cloud, BT3.9-BT12 for cloud, BT11-BT3.9 for thick and low cloud, BT11-BT12 for thin cloud, and BT6.7-BT11 for clear sky detection—are effective in detecting clouds, there are some problems. Table 3 shows that many cloudy scenes are misidentified as clear, and some clear scenes are misidentified as cloudy. There is a variety of possible reasons for these differences.

For the BT6.7 test, as shown in Fig. 4(a), the brightness temperature for cloudy cases is generally lower than of the BT for clear cases. With temperature inversions in the Arctic at night, there is little temperature difference between the clouds and the surface. It is therefore difficult to identify clouds from clear using a single threshold. Overall, only a few cloudy cases can be reliably detected using this test.

For the BT3.9-BT12 test for detecting high cloud, if the threshold is 4 K (the current value), then only the high cloud with optical thickness between 1.0 and 3.0 can be identified. The BT11-BT3.9 test can be used to detect very thick, high water cloud, but it is not useful for detecting very thick, high ice cloud. Although the threshold can be adjusted somewhat, still, very thin cloud, water cloud with optical thickness 3.0–10.0, and very thick ice cloud cannot be identified.

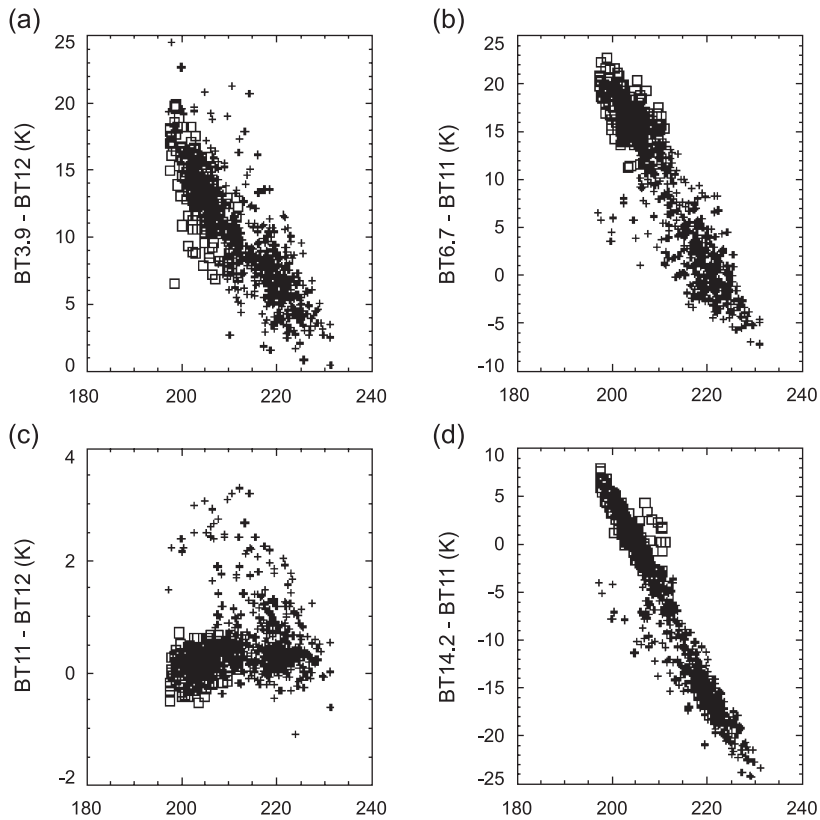

Fig. 5. Observed brightness temperature differences for (a) 3.9–12, (b) 6.7–11, (c) 11–12, and (d) 14.2–11 μm, as a function of the 11-μm brightness temperature for cloudy (+) and clear (□) cases, as determined from radar/lidar data over the Antarctic at night.

Concerning the BT11-BT3.9 low-cloud test, if we set the threshold at 0.5, then very thin, low cloud, very thick, low ice cloud and very thick, low-water cloud with effective radii larger than 20 μm cannot be identified as cloud based on simulation in Fig. 2. As shown in Fig. 4(c) and (d), we can identify many cloud cases from clear cases using the BT3.9-BT12 and BT11-BT3.9 tests, but still, many cloudy cases are misidentified as clear. For the BT3.9-BT12 and BT11-BT3.9 tests, the misidentification occurs when BT11 is between 235 and 255 K.

When temperatures are very low, BT3.9 is not very accurate due to the lower temperature and higher instrument noise; hence, under these conditions, BT3.9-BT12 is not useful. As shown in Fig. 5(a), BT3.9-BT12 at the South Pole under clear conditions at night is not separable from the BT3.9-BT12 under cloudy conditions at night. The reason for this might be too much noise at 3.9 μm, causing the test to fail. In the presence of low cloud, the brightness temperature increases, which decreases the noise at 3.9 μm. BT3.9-BT12 is larger under clear conditions than under cloudy conditions. The same situation is found in Fig. 4(c), when BT11 is very low.

In some cases, BT3.9-BT12 is large under clear conditions, even when the temperature is not particularly low. To explore the reason for this, brightness temperature differences were simulated. The temperature profile in Fig. 6(a) is changed by increasing the temperature around the inversion top by 5 (Fig. 6(d)) and 10 K (Fig. 6(g)). BT3.9-BT12 is simulated as a function of relative humidity of the atmospheric layer below inversion top and satellite-scanning angle (Fig. 6(b), (e), and (h)). We find that BT3.9-BT12 increases with increasing satellite scanning angle, increasing relative humidity below inversion top and increasing inversion strength (temperature difference across the inversion). When the inversion strength is large, the relative humidity is high and satellite scanning angle is large, as shown in Fig. 6(h). BT3.9-BT12 is generally larger than the threshold currently used, which leads to incorrectly identifying clear pixels as cloudy.

A single threshold of 10 K is used for the BT6.7-BT11 clear test at night for both the Antarctic and Arctic. From Figs. 4(b) and 5(b), this test identifies some cloud as clear in Antarctica but not in the Arctic. The reason why no nighttime clear is misidentified as cloud in Antarctica (Table 2) is that all the clear cases, plus some cloudy cases, are restored to clear by this test (Fig. 5(b)).

4. Improvements to the current algorithm

The most significant improvement to the current algorithm involves the use of the 7.2-μm water vapor band.

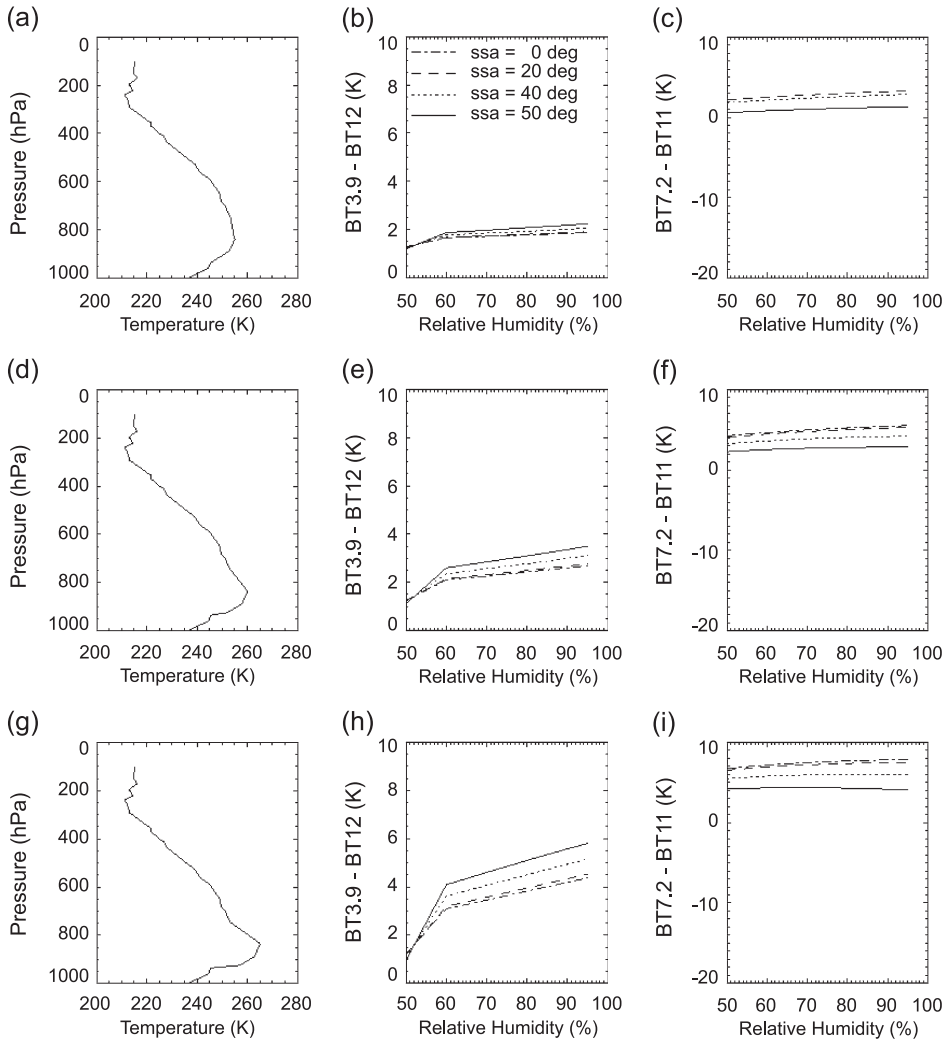

Fig. 6. Simulations of the 3.9–12 and 7.2–11 μm brightness temperature differences as a function of relative humidity for three temperature profiles. Simulated values are given for sensor scan angles (ssa) of 0°, 20°, 40°, and 50°.

Under clear-sky conditions, the brightness temperature 7.2 μm is sensitive to temperatures near 800 hPa (Fig. 1), although the radiation at 11 μm originates primarily from the surface. Therefore, BT7.2-BT11 is related to the temperature difference between the 800 hPa layer and the surface. For the Streamer Arctic summer profile with no inversion, BT7.2-BT11 is approximately −20 K. When an inversion is present, temperature and water vapor amounts are typically low, and the temperature difference between 800 hPa and the surface is small. In such conditions, BT7.2-BT11 is near −2 K, as shown in Fig. 7.

BT11 is strongly affected by low clouds and is largely a function of the cloud temperature. This is less true for BT7.2, in part due to the lower imaginary index of refraction and in part due to its broader and higher vertical weighting function. As low-cloud optical thickness increases, more radiation at 11 μm comes from the warmer cloud top instead of surface, which leads to a decreasing BT7.2-BT11. For thick, low cloud, BT7.2-BT11 does not change substantially with increasing optical depth and has a value less than that for clear conditions because of stronger absorption above the cloud top at 7.2 μm. For a high cloud, the radiation contribution at both 7.2 and 11 μm comes more from the colder cloud top and less from the warmer layers below the cloud, and the proportion of radiation from the colder cloud top is higher at 11 μm than at 7.2 μm; hence, BT7.2-BT11 is larger than under clear conditions.

Given that BT7.2-BT11 is larger for clear conditions with a temperature inversion than for low and middle clouds, a threshold could be used to distinguish clear from cloudy scenes. A pixel is labeled as cloudy when the BT7.2-BT11 is less than the threshold. This test only works when there is a temperature inversion; hence, we need to find a test to determine if an inversion is present. We use matched radiosonde and MODIS data at eight Arctic and three Antarctic meteorological stations with low surface elevations to calculate the BT11 change with inversion strength under clear conditions. Fig. 8 shows that BT11 decreases with increasing inversion strength, and when BT11 is less than 250 K, it is likely that an

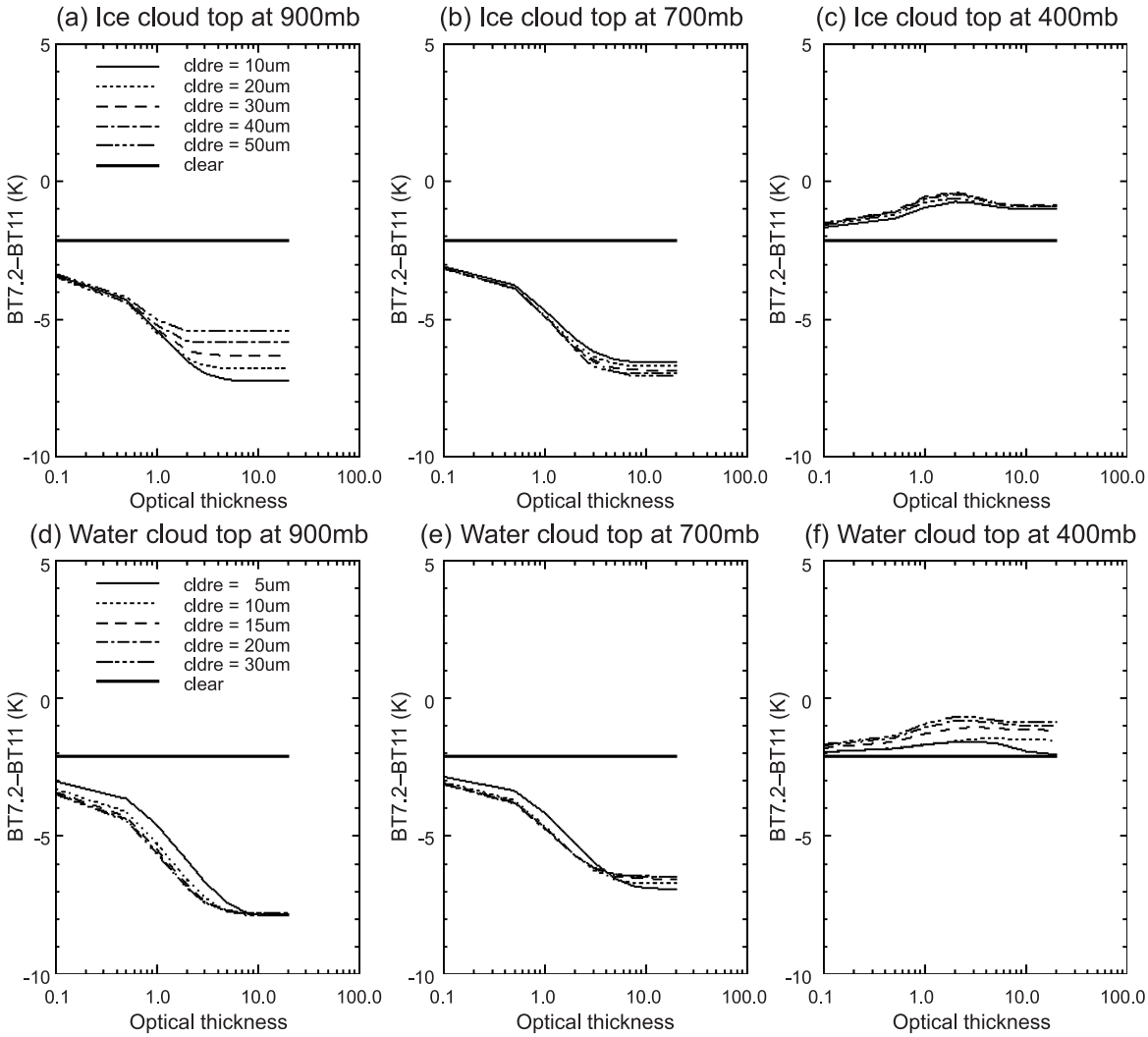

Fig. 7. Simulations of BT7.2-BT11 for ice cloud with the cloud top at (a) 900, (b) 700, and (c) 400 hPa for different ice cloud radii (cldre), and for water cloud with the cloud top at (d) 900, (e) 700, and (f) 400 hPa for different water cloud radii (cldre). An Arctic winter mean profile was used in the calculations. The temperatures at surface, 900, 700, and 400 hPa are 242, 250, 247, and 223 K, respectively.

inversion is present. Therefore, when the observed BT11 is lower than 250 K, the BT7.2-BT11 cloud detection test is applied.

To determine the threshold of BT7.2-BT11 cloud test, the range of BT7.2-BT11 under clear conditions needs to be determined. From Fig. 7(a)–(f), the range is approximately − 2 K. In Fig. 4(f), which shows BT7.2-BT11 as a function of BT11 under clear and cloudy conditions, most clear cases are easily separated from cloudy when BT11 is less than 250 K. Under clear conditions, water vapor content increases with increasing BT11, and inversion strength decreases; hence, BT7.2-BT11 also decreases. These results suggest a series of thresholds based on BT11 for the BT7.2-BT11 cloud test. The thresholds are 3, − 2, and − 5 K when BT11 is less 220, 245, and 250 K, respectively. The thresholds for other values of BT11 are linearly interpolated. A pixel is labeled as cloudy when the observed BT7.2-BT11 is less than the threshold.

The BT6.7-BT11 clear detection test works well on the Antarctic plateau, but poorly in the Arctic, where the inversion top is usually lower than 700 hPa. With a weighting function peak near 800 hPa, the 7.2 μm band can be used as a clear test in the same manner as the 6.7 μm band, with the advantage that it can detect weaker and lower level inversions. The BT7.2-BT11 clear test is used to restore the clear pixels in the Arctic and low elevation areas of the Antarctic, where a pixel is labeled as clear when the observed BT7.2-BT11 is larger than 5 K. An advantage of this test concerns the BT3.9-BT12 cloud test, which sometimes produces false cloud, as discussed earlier. When this occurs, BT7.2-BT11 is typically larger than the clear detection threshold, as shown in Fig. 6(i), so that the BT7.2-BT11 clear detection test corrects the error in the BT3.9-BT12 test.

From the simulation in Fig. 2, a BT11-BT3.9 test for detecting low clouds is very sensitive to the threshold

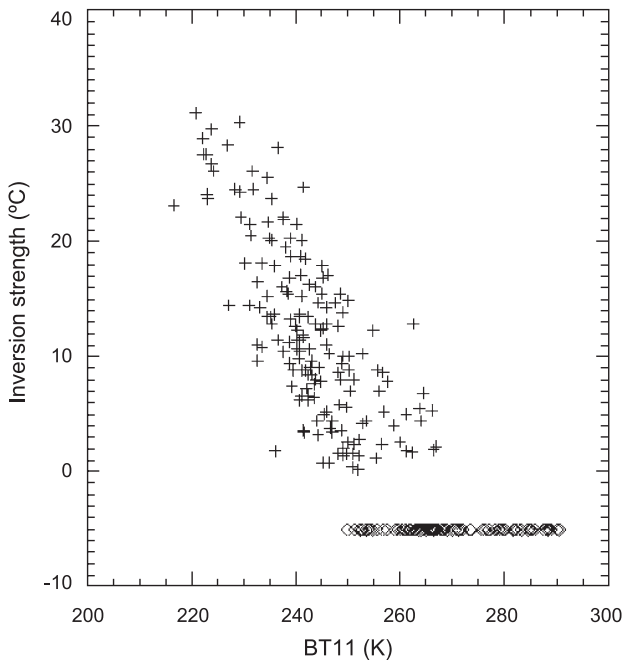

Fig. 8. The 11-μm brightness temperature as a function of inversion strength. Diamonds indicate cases with no temperature inversion.

selection, especially in the case of ice cloud. In the current MODIS cloud mask algorithm, a single threshold is used. To determine the best threshold for this test, we base our new threshold on both simulations and observations. In Fig. 9, BT11-BT3.9 is simulated as a function of BT11 under clear conditions at night using radiosonde data from Arctic and Antarctic stations with low surface elevations. BT11-BT3.9 increases with increasing BT11, also noted in the observed data given in Fig. 4(d). Therefore, in the modified MODIS cloud mask algorithm, the BT11-BT3.9 test utilizes a series of thresholds based on BT11. The thresholds are −0.9 K when BT11 is less than or equal to 235 K and 0.5 K when BT11 is 265 K or higher. The thresholds between are linearly interpolated based. A pixel is labeled as cloudy when the observed BT11-BT3.9 is larger than the threshold.

The BT11-BT12 cloud detection test is not used when the surface is snow in the current cloud mask algorithm. In the modified algorithm, the test is applied to all conditions, including snow and ice. The thresholds for this test are taken from Key (2002), who extended the Saunders and Kriebel (1988) values to very low temperatures for polar AVHRR data (Key, 2002).

The BT3.9-BT12 cloud detection test fails in Antarctic. A new cloud detection test, BT14.2-BT11, can be used to replace BT3.9-BT12 over the Antarctic plateau under very cold conditions. The basis for the BT14.2-BT11 test is similar to that for the BT7.2-BT11 test. In Antarctica, the surface altitude is very high, and water vapor amounts are low; hence, the 7.2-μm band "sees" the surface. The weighting function peak of the 14.2-μm band is near 400 hPa, hence, the 14.2-μm band data can be used in the same way as the 7.2-μm band. When the observed BT14.2-BT11 is less than the prescribed threshold of −3 K, the pixel is labeled cloudy.

4.1. Threshold sensitivity

The thresholds for each test are based on model simulations (Figs. 2, 6, 7, and 9) and real observations (Figs. 4 and 5). In the determination of threshold values, two-thirds of the cloud cases and two-thirds of the clear cases were randomly selected as the "training" data set, with the remaining cases used as the test data set. Very similar thresholds and misidentification rates occurred for different random samples. The final thresholds were derived with the entire data set.

Given the sparsity of surface-based radar and lidar data, it is difficult, if not impossible, to derive thresholds that are valid for all aspects of the complex environment in the polar regions, i.e., the broad range in surface elevation, multiple surface types, and variable lower tropospheric temperature structure. How sensitive is the cloud detection to changes in the thresholds? To test the stability of the thresholds, one-third of the cloud cases and one-third of the clear cases were randomly selected, and the final thresholds were applied to determine the misclassification rate. This sampling was repeated 100 times. The bias and standard deviation of misclassification rate of cloud as clear for the Arctic were −0.5% and 1.9%, respectively; the bias and standard deviation of misclassification rate of clear as cloud were 0.3% and 2.5%, respectively. The bias and standard deviation of misclassification rate of cloud as clear for the Antarctic were −0.2% and 1.1%, respectively; the bias and standard deviation of misclassification rate of clear as cloud were −0.2% and 1.7%, respectively.

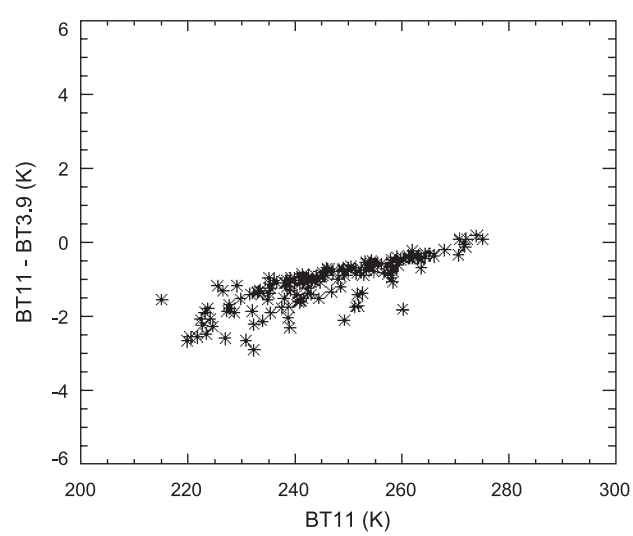

Fig. 9. The 11−3.9 μm brightness temperature difference as a function of the 11-μm brightness temperature under clear conditions at night.

Table 7
Cloud and clear test thresholds in Arctic and Antarctic

	Test	BT11-dependent threshold?	Threshold (BT11)	
Arctic	BT7.2-BT11 cloud test	Yes	3 K (≤220 K), −2 K (≤245 K), −5 K(≤250 K)	Cloud if less than threshold
	BT7.2-BT11 clear test	No	5 K	Clear if larger than threshold
	BT11-BT3.9 cloud test	Yes	−0.9 K (≤235 K), 0.5 K(≥265 K)	Cloud if larger than threshold
Antarctic	BT14.2-BT11 cloud test	No	−3 K	Cloud if less than threshold

For the BT11-dependent threshold, values between different BT11s are linearly interpolated.

To test the sensitivity of the cloud detection to the thresholds, increments of ±0.1 K were added to the thresholds of the BT11-BT7.2 cloud test, the BT7.2-BT11 clear test, the BT11-BT3.9 cloud test in Arctic, and the BT14.2-BT11 cloud test in Antarctic. Most of these shifts produce less than 0.5% change to the misclassification rates; that is, the results are relatively insensitive to small changes in the thresholds. The thresholds for the new and modified tests are provided in Table 7.

5. Application of the new algorithm

A comparison of results for the current and revised MODIS cloud mask in the Arctic and Antarctic at night is given in Table 6. In the Arctic, 16.3% of the clouds identified by radar/lidar are misidentified as clear by the modified MODIS cloud mask; 8.6% of the clear identified by radar/lidar is misidentified as cloud by the modified MODIS cloud mask. Compared with values of 44.2% and 8.1% from the current MODIS algorithm, this is a significant improvement. In the Antarctic, 2.7% of the cloud identified by radar/lidar is misidentified as clear by MODIS cloud mask; 3.7% of the clear identified by radar/lidar is misidentified as cloud by MODIS cloud mask. Corresponding values for the current cloud mask are 19.8% and 0.0%, respectively. The effects of cloud height and the number of cloud layers on cloud detection with the new and modified tests are given in Tables 4 and 5, where the numbers in parentheses are the results after the modified cloud mask algorithm is applied. We find that the cloud detection ability improved for one-layer and multilayer, as well as low, middle, and high, clouds.

An example of the application of the cloud mask algorithms is shown in Fig. 10 for January 1, 2003, at 15:25 UTC. Fig. 10(a) is a MODIS three-band composite of the 3.9- (red), 11- (green), and 12-μm bands (blue). Fig. 10(b) shows the current MODIS cloud mask, and Fig. 10(c) is the enhanced MODIS cloud mask including the modified and new tests. In the top portion of the image is cloud over sea ice. Only part of the cloud is detected with the current cloud mask, while almost the entire cloud is shown in the new cloud mask. In the middle portion of the image, the current cloud mask detects part of the cloud, but the new cloud mask identifies the majority of the cloudy area. There are also differences in the lower central portion of the image. The modified cloud mask finds more cloud than the current mask. In the bottom right corner of the image is clear sky.

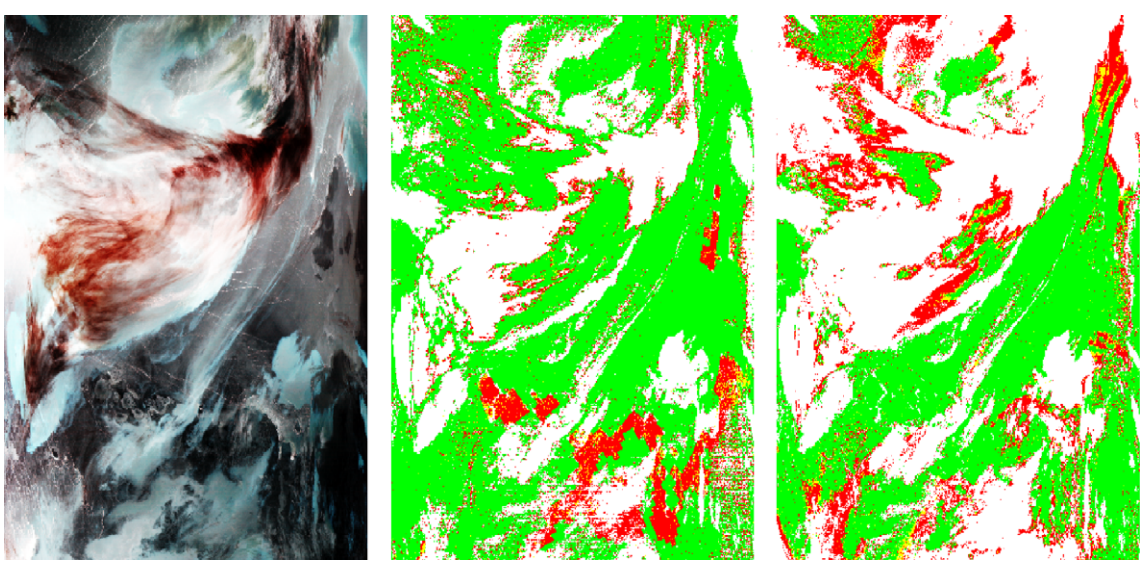

Fig. 10. An application of the current (middle) and new (right) MODIS cloud mask. Green is "confident clear", red is "probably clear", blue is "uncertain", and white is "cloudy". The left panel is a composite image of the MODIS channels 3.9 (red), 11 (green), and 12 (blue) μm. The absence of the irregular red band in the lower, middle portion of the center image from the new cloud mask (right) is due to the improvement in the surface type determination, which is not discussed in this paper.

The current cloud mask detects this as cloud due to a failure of the BT3.9-BT12 test under very cold conditions, but the enhanced cloud mask restores this to clear with the application of the BT7.2-BT11 clear test. In the middle right portion of the image is very thin cloud, which neither cloud mask detects correctly.

6. Comparison of MODIS and AVHRR cloud mask results

MODIS has all the channels that AVHRR has, which makes the comparison of MODIS and AVHRR cloud mask results possible. All the AVHRR nighttime polar cloud detection tests, including the BT3.9-BT12, BT11-BT3.9, and BT11-BT12 cloud tests, are performed using the same MODIS channel. The comparison results are shown in Table 6. The misidentification rates of cloud as clear and clear as cloud are 38.1% and 5.7%, respectively, in Arctic for AVHRR, compared with 16.3% and 8.6% for MODIS. The misidentification rates of cloud as clear and clear as cloud are 5.5% and 100.0% in Antarctic for AVHRR, compared with 2.7% and 3.7% for MODIS. The large difference between the AVHRR and MODIS misidentification rate of clear as cloud in the Antarctic is a result of the AVHRR not having a water vapor channel for clear restoral. The relatively low precision of the AVHRR 3.7-μm channel at low temperatures may also play a role.

These results are also relevant to the Visible/Infrared Imager/Radiometer Suite (VIIRS) on the future National Polar-orbiting Operational Environmental Satellite System (NPOESS). The current VIIRS specification does not include carbon dioxide or water vapor channels (this may change). Without them, its performance for polar cloud detection will be similar to that of the AVHRR, although some improvement should be expected, given its higher radiometric accuracy and channels at 1.38 and 1.6 μm.

7. Conclusions

The current MODIS cloud mask algorithm works well in the polar regions during the daytime, except over Antarctica, where false cloud detection (clear scenes labeled as cloudy) is occasionally a problem. The algorithm misidentifies much cloud in the polar regions at night, as determined using radar and lidar data at two locations in the Arctic and one in the Antarctic.

In an attempt to improve cloud detection at night, radiative transfer simulations and radar/lidar data were used to evaluate the current spectral tests and to explore new tests. New cloud tests utilizing the 7.2-μm water vapor band and the 14.2-μm carbon dioxide band can detect much more cloud when used with the current cloud tests. A clear test using the 7.2-μm band performs better than the original clear test based on the 6.7 μm band, being able to detect the weaker inversions characteristic of the Arctic and low altitude areas of the Antarctic. Other cloud tests have been modified, in particular, the test utilizing the 3.9-μm band. The new tests and modifications provide a significantly more accurate cloud detection procedure, where the misidentification of cloud as clear decreases from 44.2% to 16.3% at the two Arctic stations, and from 19.8% to 2.7% at the Antarctic station. Despite the dramatic improvement in nighttime cloud detection that these new tests provide, there are cases where the new and modified tests fail. These are primarily for very thin clouds and for weak temperature inversions with surface temperatures less than 250 K. A comparison between MODIS and AVHRR shows that MODIS nighttime polar cloud detection is superior to that of the AVHRR.

Acknowledgements

This research was supported by NASA grant NAS5-31367, NSF grant OPP-0240827, the NOAA SEARCH program, and the Integrated Program Office. Surface-based cloud radar and lidar data were provided through the Department of Energy Atmospheric Radiation Measurement program and the NOAA Climate Monitoring and Diagnostics Laboratory. We thank the MPLNET for its effort in establishing and maintaining the South Pole sites. The views, opinions, and findings contained in this report are those of the author(s) and should not be construed as an official National Oceanic and Atmospheric Administration or U.S. Government position, policy, or decision.

References

Ackerman, S. A. (1996). Global satellite observations of negative brightness temperature differences between 11 and 6.7 μm. *Journal of the Atmospheric Sciences*, *53*, 2803–2812.

Ackerman, S. A., Strabala, K. I., Menzel, W. P., Frey, R. A., Moeller, C. C., & Gumley, L. E. (1998). Discriminating clear-sky from clouds with MODIS. *Journal of Geophysical Research*, *103* (D24), 32141.

Berendes, A. T., Berendes, D., Welch, M. R., Dutton, G. E., Uttal, T., & Clothiaux, E. (2004). Cloud cover comparisons of the MODIS daytime cloud mask with surface instruments at the north slope of Alaska ARM site (Accepted by IEEE Transactions on Geoscience and Remote Sensing).

Campbell, J. R., Hlavka, D. L., Welton, E. J., Flynn, C. J., Turner, D. D., Spinhirne, J. D., Scott, V. S., & Hwang, I. H. (2002). Full-time, eye-safe cloud and aerosol lidar observation at atmospheric radiation measurement program sites: Instrument and data processing. *Journal of Atmospheric and Oceanic Technology*, *19*, 431–442.

Clothiaux, E. E., Ackerman, T. P., Mace, G. G., Moran, K. P., Marchand, R. T., Miller, M. A., & Martner, B. E. (2000). Objective determination of cloud heights and radar reflectivities using a combination of active remote sensors at the ARM CART sites. *Journal of Applied Meteorology*, *39*, 645–665.

Curry, J. A., Rossow, W. B., Randall, D., & Schramm, J. L. (1996). Overview of Arctic cloud and radiation characteristics. *Journal of Climate*, *9*, 1731–1764.

Ebert, E. (1989). Analysis of polar clouds from satellite imagery using

pattern recognition and a statistical cloud analysis scheme. *Journal of Applied Meteorology*, *28*, 382–399.

Gao, B. -C., Han, W., Tsay, S. C., & Larsen, N. F. (1998). Cloud detection over the Arctic region using airborne imaging spectrometer data during the daytime. *Journal of Applied Meteorology*, *37*, 1421–1429.

Inoue, T. (1987a). A cloud type classification with NOAA 7 split-window measurements. *Journal of Geophysical Research*, *92*, 3991–4000.

Inoue, T. (1987b). *The clouds and NOAA-7 AVHRR split window, report of the ISCCP workshop on cloud algorithms in the polar regions.* Tokyo, Japan, 19–21 August 1986, Rep. WCP-131, WMO/TD-170, Geneva.

Intrieri, J. M., Shupe, M. D., Uttal, T., & McCarty, B. J. (2002). An annual cycle of Arctic cloud characteristics observed by radar and lidar at SHEBA. *Journal of Geophysical Research*, *107*, 8030 (10.1029/2000JC000423) .

Kadosaki, G., Yamanouchi, T., & Hirasawa, N. (2002). Temperature dependence of brightness temperature difference of AVHRR infrared split window channels in the Antarctic. *Polar Meteorology and Glaciology*, *16*, 106–115.

Key, J. (1990). Cloud cover analysis with Arctic advanced very high resolution radiometer data: 2. Classification with spectral and textural measures. *Journal of Geophysical Research*, *95*, 7661–7675.

Key, J. (2002). The cloud and surface parameter retrieval (CASPR) system for polar AVHRR. Madison, WI: Cooperative Institute for Meteorological Satellite Studies, University of Wisconsin (59 pp).

Key, J., & Barry, R. G. (1989). Cloud cover analysis with Arctic AVHRR data: 1. Cloud detection. *Journal of Geophysical Research*, *94*, 18521–18535.

Key, J., Maslanik, J. A., & Schweiger, A. J. (1989). Classification of merged AVHRR and SMMR Arctic data with neutral networks. *Photogrammetric Engineering and Remote Sensing*, *55*, 1331–1338.

Key, J., & Schweiger, A. J. (1998). Tools for atmospheric radiative transfer: Streamer and FluxNet. *Computers & Geosciences*, *24* (5), 443–451.

King, M. D., Menzel, W. P., Kaufman, Y. J., Tanré, D., Gao, B. C., Platnick, S., Ackerman, S. A., Remer, L. A., Pincus, R., & Hubanks, P. A. (2003). Cloud and aerosol properties, precipitable water, and profiles of temperature and humidity from MODIS. *IEEE Transactions on Geoscience and Remote Sensing*, *41*, 442–458.

Lubin, D., & Morrow, E. (1998). Evaluation of an AVHRR cloud detection and classification method over the central Arctic ocean. *Journal of Applied Meteorology*, *37*, 166–183.

Minnis, P., Doelling, D. R., Chakrapani, V., Spangenberg, D. A., Nguyen, L., Palikonda, R., Uttal, T., Shupe, M., & Arduini, R. F. (2001). Cloud coverage and height during FIRE-ACE derived from AVHRR data. *Journal of Geophysical Research*, *106*, 15215–15232.

Platnick, S., King, M. D., Ackerman, S. A., Menzel, W. P., Baum, B. A., Riédi, J. C., & Frey, R. A. (2003). The MODIS cloud products: Algorithms and examples from Terra. *IEEE Transactions on Geoscience and Remote Sensing*, *41*, 459–473.

Ray, P. (1972). Broadband complex refractive indices of ice and water. *Applied Optics*, *11*, 1836–1844.

Rossow, W. B., & Garder, L. C. (1993). Cloud detection using satellite measurements of infrared and visible radiances for ISCCP. *Journal of Climate*, *6*, 2341–2369.

Rossow, W. B., & Schiffer, R. A. (1991). ISCCP cloud data products. *Bulletin of the American Meteorological Society*, *72*, 2–20.

Rossow, W. B., & Schiffer, R. A. (1999). Advances in understanding clouds from ISCCP. *Bulletin of the American Meteorological Society*, *80*, 2261–2287.

Rossow, W. B., Walker, A. W., Garder, L. C. (1993). Comparison of ISCCP and other cloud amounts. *Journal of Climate*, *6*, 2394–2418.

Saunders, R. W., & Kriebel, K. T. (1988). An improved method for detecting clear sky and cloudy radiances from AVHRR radiances. *Int. J. Remote Sensing*, *9*, 123–150.

Schweiger, A. J., Lindsay, R. W., Key, J. R., & Francis, J. A. (1999). Arctic clouds in multi-year satellite data sets. *Geophysical Research Letters*, *26*, 1845–1848.

Segelstein, D. (1981). *The complex refractive index of water*. MS thesis, University of Missouri-Kansas City.

Spangenberg, D. A., Chakrapani, V., Doelling, D. R., Minnis, P., & Arduini, R. F. (2001). Development of an automated arctic cloud mask using clear-sky satellite observations taken over the SHEBA and ARM-NSA sites. In: Proc. AMS 6th Conf. On Polar Meteorology and Oceanography, San Diego, CA, May 14–18.

Spangenberg, D. A., Doelling, D. R., Chakrapani, V., Minnis, P., & Uttal, T. (2002). Nighttime cloud detection over the Arctic using AVHRR data. In: Proc. 12th ARM Science Team Meeting, St. Petersburg, FL, April 8–12.

Strabala, K. I., Ackerman, S. A., & Menzel, W. P. (1994). Cloud properties inferred from 8–12 micron data. *Journal of Applied Meteorology*, *33*, 212–229.

Warren, S. G. (1984). Optical constants of ice from the ultraviolet to the microwave. *Appl. Optics*, *23*, 1206–1225.

Welch, R. M., Sengupta, S. K., & Chen, D. W. (1988). Cloud field classification based upon high spatial resolution textural features: Part I. Gray level co-occurrence matrix approach. *Journal of Geophysical Research*, *93*, 12663–12681.

Welch, R. M., Kuo, K. S., & Sengupta, S. K. (1990). Cloud and surface textural features in polar regions. *IEEE Transactions on Geoscience and Remote Sensing*, *28*, 520–528.

Welch, R. M., Sengupta, S. K., Goroch, A. K., Rabindra, R., Rangaraj, N., & Navar, M. S. (1992). Polar cloud and surface classification using AVHRR imagery: An intercomparison of methods. *Journal of Applied Meteorology*, *31*, 405–420.

Yamanouchi, T., Suzuki, K., & Kawaguchi, S. (1987). Detection of clouds in Antarctica from infrared multispectral data of AVHRR. *Journal of the Meteorological Society of Japan*, *65*, 949–962.